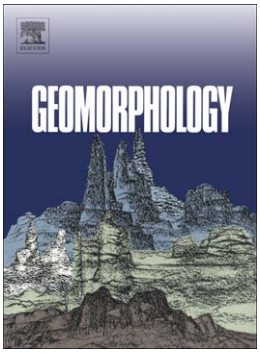

Crack propagation by differential insolation on desert surface clasts

John E. Moores, Jon D. Pelletier, Peter H. Smith

PII: S0169-555X(08)00205-5
DOI: doi: 10.1016/j.geomorph.2008.05.012
Reference: GEOMOR 2649

To appear in: *Geomorphology*

Received date: 17 January 2008
Revised date: 14 May 2008
Accepted date: 14 May 2008

Please cite this article as: Moores, John E., Pelletier, Jon D., Smith, Peter H., Crack propagation by differential insolation on desert surface clasts, *Geomorphology* (2008), doi: 10.1016/j.geomorph.2008.05.012

Crack propagation by differential insolation on desert surface clasts

John E. Moores*, Jon D. Pelletier[1], Peter H. Smith[2]

University of Arizona, Department of Planetary Sciences
1629 E University Blvd., Tucson, AZ 85721-0092, USA

*Corresponding author. Tel.: +1 520-626-4769; Fax: +1 520-626-1973;
E-mail: jmoores@lpl.arizona.edu.
[1]E-mail: jdpellet@email.arizona.edu.
[2]E-mail: psmith@lpl.arizona.edu.

Abstract

In the southwest U.S., cracks in alluvial fan surface clasts have a preferred orientation independent of rock fabric and shape. In this paper, we show that differential insolation of incipient cracks of random orientations predicts a distribution of crack orientations consistent with field observations. In this model, crack growth by hydration and/or thermal weathering is primarily a function of local water content at the crack tip. Crack tips that experience minimal solar insolation maintain a greater average moisture and, hence, weather more rapidly than cracks that experience greater solar insolation. To show this, we used a numerical radiative transfer code to quantify the solar insolation of rectangular cracks at 35° N. latitude with a range of depths and orientations. The amount of solar energy reaching the bottom of each crack was calculated at 5-min intervals over the day for several days of the year to determine hourly, daily, seasonal, and annual energy deposition as a function of crack depth and orientation. By assuming that only crack orientations that effectively shield their interiors and minimize their water loss are able to grow, the pattern of cracks produced by the model is consistent with field observations. The annual average insolation, which controls water retention, is associated with the two primary modes of crack orientation. The effect of daily recharge by summer rains of the North American monsoon system is consistent with the observed deviations from these primary modes. Model results suggest that both the annual average insolation and the daily pattern of rainfall is recorded in the preferred crack orientations of surface clasts in the southwest U.S.

Keywords: weathering; solar insolation; desert pavement; hydrology

1. Introduction

The breakdown mechanism of surface clasts in arid environments has been a topic of debate for almost a century. A central question in this debate is whether thermal stresses or hydration weathering is the dominant processes of clast breakdown (Mabbutt, 1977). Recently, McFadden et al. (2005) documented a preferred N-S orientation in the cracks of surface clasts in deserts of the southwest U.S. with the effects of rock fabric and shape removed (Fig. 1). Because surface clasts are deposited randomly, this preferred orientation develops after clast deposition. McFadden et al. (2005) argued that this pattern provides direct evidence for the predominant role of thermally induced mechanical stresses resulting from differential heating of clasts as the sun moves across the sky during the course of a day. Other breakdown mechanisms can also be influenced, however, directly or indirectly, by solar insolation. As such, quantitatively developing and testing multiple alternative hypotheses for the factors influencing clast breakdown on desert surfaces is important.

Diurnal air temperature variations of at least 24°C are possible (Leathers et al., 1998, data for Wilcox, AZ) in near-surface desert environments, with even higher values possible within surface clasts. This variation causes surface clasts to expand and contract, generating mechanical stresses within the rock. At the scale of individual mineral grains, these stresses are the result of different thermal expansion coefficients. At larger scales, if the rock is larger then the depth of the diurnal thermal wave, stresses may build up between zones of different temperature (Simmons and Cooper, 1978). The magnitude of these thermal stresses, however, has been suggested to be generally not sufficient to fracture rocks catastrophically (Blackwelder, 1933). If rocks break down by mechanical stresses, it is most likely through repeated cycling at stresses below the failure stress of the material (Griggs, 1936). Early experiments designed to test the efficacy of this fatigue-breakdown process in very dry environments

(Griggs, 1936) were unable to detect any disintegration or crack growth even on a microscopic scale after cycling several specimens for an equivalent of 244 years of diurnal temperature cycles. Fredrich and Wong (1986), however, detected small cracks in thermally cycled materials. These results suggest that significant crack growth could occur because of thermal stresses at temperatures as low as ~ 140°C in certain crustal rocks. Studies examining the microseismic properties of thermally cycled rocks have found no clear evidence of damage done by cracking until rocks have reached 200°-400°C (Simmons and Cooper, 1978; Johnston and Toksöz, 1980; Clark et al., 1981). Changes in microseismic properties below these temperature values are largely due to outgassing of volatiles. These temperatures are all much higher then peak temperatures typically observed on desert rocks (McFadden et al., 2005).

In experiments, the situation changes once moisture is introduced. Griggs (1936) found that samples of rock that had survived the equivalent of 244 years of diurnal cycling disintegrated noticeably within 10 days of cycling (equivalent to about 2-3 years of exposure) when cooled with a mist of water (Griggs, 1936). Barton also found a correlation between the presence of moisture and the degree of disintegration of ancient monuments in Egypt. Here, areas with higher relative humidity and rainfall but equivalent insolation exhibited greatly enhanced breakdown rates (Barton, 1916, 1938). This is consistent with the observation that the oldest surface clasts on Earth, as determined by cosmic ray exposure ages, are found in the most hyperarid deserts (Dunai et al., 2005), suggesting that aridity is inversely correlated with clast breakdown rate.

These results suggest that the moisture concentration in clasts is the limiting factor in clast breakdown. Clast breakdown occurs by a complex combination of hydration weathering and thermally induced mechanical processes. Hydration weathering in this context refers to any process by which water acts as

a catalyst for rock breakdown. including salt weathering, dissolution, freeze-thaw microfracturing, and granular disintegration. In all these processes, breakdown is driven either directly or indirectly by the moisture concentration of the rock. As such, a better understanding of rock breakdown requires that the recharge and discharge of moisture into surface clasts be quantified within a process-based framework. Because cracks offer partial shielding from solar insolation, they act as locations of enhanced water retention by the rock. In this way, crack orientations that offer preferential shielding from solar insolation will retain the most water and hence can be expected to grow at the expense of cracks with other orientations.

2. Model description

2.1. Introduction

Given that water must be present in order to break down rock, then differential insolation of cracks must be considered. The reason for this is that cracks, in general, represent areas of a rock in which water can be retained for longer times then directly on the surface because their concave geometry provides a low point in which water can accumulate, they shield their interiors from solar insolation, and (if they are deep enough) they can shield their interiors from the daily thermal wave penetrating into the rock from the surface. As such, cracks oriented to receive more insolation will evaporate more water from their interiors and will bake out entirely before cracks of other orientations. This means that if water is required for a crack to grow, those cracks that preserve their internal water for the longest period of time will grow preferentially. These preferential cracks will be those with the lowest amount of insolation over the timescales relevant to crack formation.

From where do these cracks arise? No real-world material is a perfect single crystal and, as such, any rock will have an abundance of grain boundaries, defects, and mechanical microcracks from striking other rocks. In general, these flaws in the surface of the material should be randomly oriented, and any cracks that follow the fabric of the rock have been filtered out of Fig. 1 by McFadden et al. (2005). Because any surface clast will have a large number of these randomly oriented microcracks, it will be reasonably assumed that all orientations are present initially. Not only will these microcracks differ in direction, but they will also differ in size and in their depth-to-width ratios. This last variation is not entirely random as more shallow cracks are to be expected compared to deeper cracks. As such, cracks of all orientations and depth-to-width ratios will be considered in the model scenario.

2.2. Modeling differential insolation

The solar insolation within the cracks is modeled using a plane-parallel radiative transfer code. Originally designed by Martin Tomasko to perform calculations in the atmosphere of Titan (Tomasko et al., 2005), the code has been successfully adapted to Mars (see Sprague et al., 2006) and to the Earth in order to perform calibration calculations for the Phoenix Lidar instrument. For the purposes of this model, given the low optical depths, the clear-sky nature of arid regions, and the isotropy of scattering in the terrestrial atmosphere, we consider only the attenuated direct beam and not the diffuse sky irradiance. As such, the modeled atmosphere contains no Mie scattering centers (dust particles, clouds, or other aerosols) and a sea-level standard 1 bar of rayleigh scattering gas with the properties given by the ASTM G173-03 1.5 airmass standard (ASTM, 2003).

The wavelength range of study, 400 to 980 nm, comes from the extent under which the Tomasko code is well tested and comprises 70% of the shortwave energy received at the surface of the Earth. Only visible

light was modeled, as many rocks are dark and absorb optimally within the visible portion of the spectrum. Short-wave infrared is also highly directional and will produce the same patterns as visible light.

The cracks themselves are modeled as rectangular troughs with flat bottoms and sides, as in Moores et al. (2007) and shown schematically in Fig. 2. The assumption has been made that the cracks are found on a flat, horizontal surface, both for simplicity and because this orientation of crack can retain the largest amount of water. As the sun moves across the sky during the day, the model determines if it can be seen from each of 200 individual area elements located on the bottom of the trough. If the sun is not seen, the incident flux on that panel is zero for that configuration of the sun in the sky. The rock surface is considered sufficiently dark that reflections from the trench walls are not significant. The energy variations to be presented in section 3 describe the total energy received at the bottom of the trough. As such, this can be considered as characteristic of the amount of down welling radiation at a characteristic depth. Trough deepening is accomplished by deepening the floor of such a trench while keeping the cross section constant. These troughs will be described by their aspect ratios in the manner of length:width:depth.

The final piece of information required to plot the path of the sun on each day of interest is the latitude of the observer. Because this model will be tested against the orientations shown in McFadden et al. (2005), a latitude of 35° N., a typical value for the sites surveyed in this study, was chosen.

In order to build up diurnal, seasonal, and yearly variations, the model tracks the sun in the sky at 5-min intervals during the day for eight values of the solar longitude equally spaced over the year (L_S = 0° or

vernal equinox; L_S = 45°; L_S = 90° or northern summer solstice; L_S = 135°; L_S = 180° or autumnal equinox; L_S = 215°; L_S = 270° or northern winter solstice; and L_S = 315°). Intermediate values, when necessary, are obtained by interpolating between these points.

In a similar manner, rotation of the trench allowed the simulation of different crack orientations. This consisted of 90 equally spaced points between 0° (a N-S orientation) and 90° (an E-W orientation) for seasonal and annual variations. This is the frame of reference shown in all rose diagrams. As the energy received when the crack is oriented to the west of N-S is equivalent to the energy received when the crack is oriented east of north (because of the symmetry of the path of the sun in the sky on any given day), rotating the crack through 180° was not necessary except when calculations were performed within a day (diurnal variations). This allowed for finer precision in trench orientation.

2.3. Timescales of crack recharge and discharge

Before examining the distribution of energy in cracks of different orientations, the timescales of crack recharge and discharge must be considered. This will determine whether diurnal, monthly, seasonal, annual, or longer variations in insolation must be considered for each mechanism or if only a subset is necessary. The motivation for this analysis is to determine when cracks can be considered wet and when they can be considered baked out. We will show that recharge of cracks, dependant on liquid infiltration of the region near the crack tip, occurs quickly; while discharge through diffusion of water vapor is a much slower process. This section will quantify this assertion.

First, the basic parameters of the problem will be defined. A simple model will be used: the crack tip is assumed to represent an entranceway into a network of cylindrical-pore “tubes.” As such, two

parameters are required to estimate the timescale of discharge and recharge: the radius of the pore tubes and the length of the connected porosity network. Because larger pores serve as entrances to smaller pores with lower fluxes, a range of pore sizes must be considered. For typical unfractured granitic rock, observed pore radii range widely from a few nanometers (Iñigo et al., 2000) to a few tens of nanometers (Klobes et al., 1997) or even a few hundreds of nanometers to microns (Geraud et al., 1992) or larger for other volcanic and sedimentary rocks. Pore tube lengths have been determined by Schild et al. (2001) by injecting granitic samples with an acrylic resin before coring and removal. The penetration depth into the rock in these experiments was observed to be ~ 5 cm. This gives a minimum length of connected porosity because typical granitic rocks have low porosity compared to other surface clasts; as well, these pathways are highly tortuous and hence the total distance is likely to be much greater than the straight-line distance of 5 cm. For this analysis, we choose a conservative value of 10 cm to represent the pore tube length within this order of magnitude analysis.

First, let us consider the mechanism of crack recharge. When a crack is full of water, some of the liquid will be drawn into the pores by capillary action. Neglecting the height of water in the crack, the pressure differential corresponding to the capillary force acting to fill the pores can be expressed as

$$\Delta p_{Capillary} = \rho g h_{Equilibrium} = \rho g \frac{2\gamma \cos\theta}{\rho g r} \cong 1.37x10^{-4} \frac{\rho}{r} \qquad [1]$$

Where r is the radius of the capillary, and γ is the surface tension of water. The contact angle, θ, is taken to be 20°, characteristic of a typical hydrophilic surface. Because the pores are small, we can assume a laminar Poiseuille flow within the capillaries. This allows us to determine a recharge time by dividing

the mass of water that the capillary would have if entirely full by the rate of flow into the capillary, assuming that the crack represents an infinite reservoir compared to the capillary pores:

$$\tau_{\mathrm{Re}ch\mathrm{arg}e} = \frac{M_{Capillary}}{Q_{Capillary}} = \frac{\rho \Delta l \pi r^2}{\frac{\pi r^4 \Delta p}{8\eta \Delta l}} = \frac{\rho \Delta l \pi r^2}{1.37x10^{-4}\frac{\rho \pi r^3}{8\eta \Delta l}} = \frac{8\eta(\Delta l)^2}{1.37x10^{-4} r} \qquad [2]$$

In the discharge case, liquid present in the capillaries must evaporate and diffuse out of the capillary. Because the diameter of the capillaries under consideration spans the mean free path of water vapor in air of about 10^{-8} m, we must consider both molecular and Knudsen diffusion processes (in which there are more collisions of gas particles with the capillary walls then with other gas particles). In the Knudsen regime, the diffusion coefficient can be expressed as (Clifford and Hillel, 1983)

$$D_K = \frac{3}{2} r \sqrt{\frac{8TR}{\pi}} \qquad [3]$$

where R is the specific gas constant (462 $m^3/s^2 \cdot K$ for water vapor), T is the temperature (in Kelvin) and r is again the capillary radius. For pore radii larger then 10^{-8} m, the molecular diffusion coefficient for water vapor in air (fit to Appendix 3 of Gates, 1980) is used

$$D_M = 1.505x10^{-7} T - 1.991x10^{-5} \qquad [4]$$

for T in Kelvin. From this we can calculate a particle speed by approximating the diffusion equation using finite differences

$$\frac{\partial C}{\partial t} = D\frac{\partial^2 C}{\partial l^2} \Rightarrow \frac{\Delta C}{\Delta t} \approx D\frac{\Delta^2 C}{\Delta l^2} \Rightarrow \Delta t \approx \frac{\Delta l^2}{D} \qquad [5]$$

For pathways ending at the walls of the larger crack, the temperature of the crack walls and the temperature of the air in the crack is a controlling factor on the number of escaping particles. This is the result of escaping water molecules being thermalized to the same temperature as the crack over a very short length scale by striking the walls of the capillary or air molecules in the vicinity of the capillary exit. If the number of diffusing molecules exceeds the maximum allowed by the saturated vapor pressure, they will condense and flow back down into the capillary as liquid. In this way, the temperature at the surface of the crack, as dictated by the amount of solar insolation absorbed, can control the flux of escaping water from that crack. Thus, the output of the capillary is assumed to be saturated and the crack volume represents an infinite sink of humidity (i.e., relative humidity = 0% enforced at the crack/capillary boundary). The discharge time can now be written as

$$\tau_{Discharge} = \frac{M}{Q} = \frac{\rho_{liquid}\Delta l \pi r^2}{\oiint_{Capillary} v\rho_{vapor}\, dA} = \frac{\rho_{liquid}\Delta l \pi r^2}{v\rho_{vapor}^{outlet}\pi r^2} = \frac{\rho_{liquid}\Delta l}{v\rho_{vapor}^{outlet}} \qquad [6]$$

Equations [2] and [6] can now be plotted for the pore size range of interest (Fig. 3) using values for the various constants taken at 20°C. The most significant feature of this plot is the observed rolloff in the discharge rate for pores larger then a few tens of nanometers. This means that for the largest pores that represent the largest volume of water and the major pathways into the smaller pores and microcracks, recharge can not only happen very quickly (on the order of hours), but occurs much more rapidly then

crack discharge. As a result, unlike ponded water in a macroscopic crack (which will evaporate quickly from direct contact with the atmosphere), water in these pores and microcracks is stable on long timescales and will continue to recharge smaller microcracks and pores during this period. The characteristic timescale of discharge is of the order of $2x10^7$ s, or about two-thirds of a year.

This is most likely a lower bound for several reasons. First, even in the driest parts of the U.S. southwest, a relative humidity of 0% is almost never achieved in reality. Any increase in the relative humidity within the crack above 0% will tend to reduce the concentration gradient over the capillary network and reduce the rate of vapor exiting the capillary. Secondly, if the capillaries are not entirely discharged before the next recharge event, the smallest pore spaces that are the last to be filled and the last to be baked out will gradually fill up over time. Thus, progressively, a much longer timescale will be required to bake out these cracks, which will also retain a progressively larger fraction of their internal water. Also, any process that causes weathering products to accumulate within the crack will enhance this process as the pore network will be effectively lengthened and more water can be protected from the sun (this topic is briefly discussed in section 4.1).

3. Results

3.1. Insolation variations between different orientations of cracks

Fig. 4 shows the variation in insolation for a family of cracks varying only in their orientation over a single day for (panel A) a shallow crack (aspect ratio of 8:1:1) and for (panel B) a deeper crack (aspect ratio of 8:1:4). As can be seen from Fig. 4, as the crack deepens, the range of orientations over which insolation is received at any one time of day becomes progressively restricted. Also, the peak height of the insolation at any time becomes lower; this is a result of averaging over the crack bottom, the entirety

of which may not be illuminated at once for deeper cracks. This effect can also be seen in panel A of Fig. 4 in which the interplay of shadows from different sides of the crack cause a jagged curve in contrast to the sharp curve seen in panel B, in which only a small portion of the crack bottom is illuminated at any one time.

At some time during the day almost any orientation of crack may instantaneously receive the most insolation; however, upon looking at the seasonal plots (Fig. 5) for both these depths that integrate the received insolation over the course of the day, E-W cracks receive more insolation in summer and N-S cracks receive more insolation in winter. This seasonal change is due to the path of the sun in the sky. In the summer months, the maximum declination of the sun in the sky at noon is small (< 12° at 35° N.) resulting in E-W oriented cracks receiving insolation over a much greater proportion of the day then N-S oriented cracks. The opposite is true in the winter months when the sun is always in the south, favoring N-S oriented cracks over E-W cracks that remain in perpetual shadow. As the crack deepens, the proportion of the year that exhibits the “winter” behavior increases at the expense of the “summer” period.

Finally, Fig. 6 displays the relative total over the entire year. These cracks have an interesting dependence, with three different regimes in insolation depending upon the depth of the crack. The first regime (Fig. 6, panel A) is a monotonic increase with E-W oriented cracks receiving the most insolation. This is the result of a domination of the summer months in the insolation curve in which E-W cracks receive more insolation then the N-S cracks. This regime extends from the shallow end to relative depths of 1 to 1.2 units. At large crack depths, > 2.5 to 2.8 units in depth, the opposite relationship is true (Fig. 6, panel C) with N-S cracks receiving more insolation as the “winter” regime dominates. However, an

interesting crossover region exists between these two in which latitudinal effects dominate and a minimum is observed at about 35° N. of E-W (Fig. 6, panel B).

3.2. Crack growth in response to insolation variations

By examining the graphs in Figs. 4-6, minimums in insolation can be discerned in each data set that will correspond to maxima in the ability of these cracks to retain water. Based on our assumption that water is required for cracking, the orientations that correspond to these maxima should therefore indicate the directions of cracks that would be expected to grow preferentially. The insolation variations used correspond to the three timescale classifications discussed in section 3.1, sub-diurnal, diurnal to seasonal, and annual. From section 2.3, annual variations are expected to be most significant for discharge of cracks. The effect of crack recharge shall be discussed separately in section 3.3.

First, the annual variation for discharge is considered. To highlight the possible resulting crack directionality if there is a limit on the amount of water that each crack can hold, a threshold in energy has been added beyond which cracks are considered to be baked out. Results are presented in Fig. 7 for the three regimes shown in Fig. 5 (Note that the three energy thresholds used were 1.65×10^{9} J y^{-1} m^{-2}, 4.70×10^{8} J y^{-1} m^{-2}, and 1.12×10^{8} J y^{-1} m^{-2} for A, B, and C classifications, respectively; see section 4.1 for a discussion of the different values of the evaporation threshold.) The effect of the evaporation threshold is to cause N-S oriented cracks to propagate when the incipient cracks are themselves shallow as E-W cracks are permanently baked out because of the large amounts of insolation received in the summer. If the incipient cracks are deeper then 1.2 units, a second population of cracks with ENE-WSW and ESE-WNW orientations can be produced. Finally, for deep incipient cracks (3 units or more), E-W orientations are favored. Extreme examples of each case have been shown in Fig. 7 to demonstrate the

possible modes of the system. Even so, note that this is not simply a rotation of the most favoured crack direction with increasing crack depth. Analogously to the three regimes discussed in section 3 for the annual average insolation of cracks, the three peaks shown in Fig. 7 (panels A, B, and C) are the only three peaks seen in the data.

While not expected to be significant, the seasonal variation was also examined. Once cracks are permitted to respond to seasonal variations, all cracks produced are E-W oriented. The reason for this is that there is always a global minimum of insolation for all depths of crack in the wintertime at an E-W orientation. As such, all cracks will grow most easily at this time of the year if the timescale of discharge is sufficiently short to respond to this signal. Because this E-W orientation is not well expressed in the data set of McFadden et al. (2005), seasonal variations cannot be important for discharge.

Before concluding this section, it is important to point out how it is possible to reconcile the differences in insolation at different depths. For instance, considering Fig. 6, N-S orientations are favored for shallow cracks (Panel A) while for intermediate cracks (Panel B) ENE-WSW and WNW-ESE orientations are favored. Because a growing crack will become more highly favored and be more able to hold on to its internal water the deeper it gets, this begs the question that if shallow ENE-WSW and WNW-ESE cracks cannot grow, how can they ever be favored? The solution lies in the initial random distribution of cracks. Recall from section 2.1 that the assumption has been made that rocks will tend to have randomly distributed surface cracks initially that also will differ in their depth-to-width ratios. Some rocks will initially possess only slightly damaged surfaces on which shallow microcracks will dominate, while other rocks will possess more heavily damaged surfaces with deeper microcracks being more common. Thus, the initial state of the rock will determine which class of preferred orientation will

grow. If there are more rocks with shallower microcracks/surface defects then rocks with deep microcracks, there should be more examples of rocks in the shallowest crack regime, with fewer rocks in the intermediate regime and fewer still in the deep-crack regime. This is consistent with the field observations documented in Fig. 1.

3.3. Crack recharge

The secondary mode is exhibited only along an ENE-WSW axis in Fig. 1, instead of being symmetric about the N-S axis (i.e., the WNW-ESE mode is not represented) as seen in the results from section 4.3 and in Fig. 7. Because the position of the sun in the sky is symmetric about the N-S axis, it cannot be an insolation effect on a seasonal or annual timescale and must instead be a diurnal effect. This suggests a closer examination of crack recharge that, from section 2.3, is expected to be most important on an hourly to daily timescale, depending upon the largest pore size. As such, we must determine if any orientation bias will be introduced by the amount and timing of available recharge.

Section 3.1 discussed the selection bias for different crack orientations at different times of the day. As such, the diurnal pattern of precipitation is key to understanding this effect. To this end, diurnal precipitation patterns were considered for Los Alamos, NM (Bowen, 1996), a typical location near the New Mexico cluster of studied data points in McFadden et al. (2005). This data shows no significant hourly preference for precipitation for much of the year; however, in the summer months a strongly expressed peak in precipitation is exhibited at 1400. In general, the afternoons tend to be much wetter then the mornings, as is typical for convective activity in the summer time. This trend is confirmed by a second study in which the frequency of precipitation was analyzed for eight separate study areas within southern New Mexico (Tucker, 1993) at different elevations that bracket the elevations of the study

areas examined by McFadden et al. (2005) Each of these eight stations reports a peak in precipitation during the afternoon.

Which crack orientations will this favor? The most likely candidates are those orientations that receive most of their insolation in the morning, before 1400. Because these cracks will typically be shielded after precipitation has fallen, they should be able to retain this water for a longer amount of time (potentially overnight), which will allow more water to diffuse into the rock for these orientations. This can be calculated from the tables of insolation produced for the diurnal variation described in section 3. The cumulative energy received by 1320 on 6 August of any given year ($L_S \sim 135°$) as a fraction of the total energy received on 6 August is displayed in Fig. 8 for several different crack depths and orientations. For all depths, more energy is received for orientations between 90° and 180° then for orientations between 0° and 90°. This effect increases for increasing depth extending from an average 7.4% differential for an aspect ratio of 8:1:1 to 26.8% for an aspect ratio of 8:1:4. In particular, at the two orientations of 60° and 120°, much more of the daily insolation has been received at 120° by early afternoon suggesting that this orientation should be able to retain more water for a longer period as it will not be baked out significantly following precipitation. This 120° mode is precisely the mode expressed in the work of McFadden et al. (2005).

Because N-S cracks are also favored in the summer months, these should respond to the same diurnal pattern. However, because the asymmetry is less pronounced for cracks near 0° and 180° in orientation and disappears entirely for deep cracks, it should represent a lesser effect. This is a possible explanation for the 7° vector-mean offset described by McFadden et al. as cracks with orientations between 150° and

170° (NNE-SSW) are slightly favoured over cracks with orientation between 10° and 30° (NNW-SSE). This is also seen in the rose diagram after McFadden et al. (2005) in Fig. 1.

4. Discussion

4.1. Model limitations

Our goal in this paper was to quantitatively model the growth of cracks as a function of depth and orientation, assuming that crack growth correlates with moisture concentration in water-limited environments. A complete process-based understanding of clast breakdown will require that specific mechanisms (e.g., hydration weathering, thermally induced mechanical stresses, etc.) be modeled in detail at a range of scales from grain boundaries to whole rock as well as a consideration of different shapes, albedos, and minerologies. In this section, these and other model limitations will be discussed. We will argue that many of these limitations are higher order effects that will not significantly affect the results that have been derived using the model. Instead, the results of this paper clearly show that differential solar insolation exerts a first-order control on the discharge and recharge of water into rocks. To the extent that clast breakdown is controlled by moisture, therefore, differential solar insolation also exerts a first-order control on clast breakdown.

While cracking along the preferred directions exhibited in Fig. 7 represents a minimum-energy solution (i.e., maintaining water in other orientations of crack is more difficult), other factors exist that will tend to broaden or add noise to this cracking variation. Any event, such as an earthquake or landslide that is able to re-orient rocks after cracks have formed without disrupting the rock, will broaden the peak

ientations seen in Fig. 7 as small reorientations are likely more common then large reorientation events. This could be one reason for the fairly broad peaks seen in Fig. 1.

Additionally, cracks can be the result of mechanical damage caused by other rocks. McFadden et al. (2005) attempted to correct for this problem by removing fractures relating to rock shape and fabric (zones or inherent weakness in the rock). However, if a rock happened to be mechanically fractured in such a way as to escape this filter, random noise would be added to the sample as these false-positive clasts should, statistically, be randomly oriented. A similar effect is expected for nonplanar rocks. In reality, rocks in a field do not all possess a flat upper surface to present to the sun. However, the vector average of all face orientations is expected to be upwards; as such, an upward face is a reasonable approximation.

Another model uncertainty concerns the value of the threshold energy required to remove all the water from a crack, E_T. E_T is an unknown parameter that will vary according to rock type, degree of disintegration, number of open pathways, and relative humidity. For instance, the ability of surface clasts to retain water may be highly enhanced as incipient cracks deepen and the rock in the vicinity of the crack becomes more weathered. This increases the surface area on the inside of the crack and the number and size of capillary-like openings within the interior of the rock (Iñigo et al., 2000), both of which would be expected to increase E_T. As such, the value of E_T will be different even amongst different rocks in the same field. However, E_T should be the same for all incipient cracks located on the same rock, thus in the localized setting of that rock the specific value of E_T will cause either (i) all cracks to propagate equally for E_T greater than the maximum energy of all orientations in which all cracks are equally hydrated; (ii) a preference for a certain direction of crack, the case considered in

section 3.2 for which E_T is less than the maximum energy but greater than the minimum energy of all orientations and some cracks are hydrated while some are baked out; or (iii) no crack propagation at all for E_T less than the minimum energy of all orientations and all cracks are baked out.

It may seem artificial to only consider case (ii) when dealing with this parameter. However, when examining rocks in the field, rocks with all cracks propagating equally (case i) will appear to have disintegrating crusts, while rocks on which cracks cannot propagate (case iii) will appear pristine. In examining the orientation of rocks with a predominant crack, these other two cases will be ignored because of the sampling method. After all, the large-number statistics of McFadden et al. give average trends in orientation and are not meant to imply that every single rock in a given field is fractured or fractured in the same way, nor that any one rock has more then one predominant fracture direction. As such, because we are describing tendencies that encourage the formation of a predominant crack, the selection of E_T to lie in the range that produces aligned cracks simply accounts for the observational selectivity inherent in building up a database of rocks with aligned cracks by the simple fact of rightly ignoring rocks without aligned cracks.

As a result of this analysis, albedo is not expected to be a controlling factor, as albedo changes only the threshold energy by changing the efficiency of heat absorption. Similarly, absorption of heat at different levels of a clast from minerologies of varying translucence (Hall et al., 2008) as well as different thermal diffusivities for individual grains would also affect this threshold value, but not the overall pattern of cracking. Instead, the energy threshold change from changing the mineralogy of a clast may push it into zones where the (i) and (iii) cases dominate preventing a cracking pattern from occurring at all. If the clast remains within the zone governed by case (ii), the rate or efficiency of crack formation may

change; however, recall that the patterns themselves are not dependant on this rate of crack propagation. Albedo also changes with the angle of illumination for many materials (e.g., Hapke, 1993) that would have an effect beyond a simple change in E_T. This has been neglected in our analysis as this variation for many materials is small compared with the magnitude of the mean albedo, neglecting specular reflection.

We would like to emphasize that this model is a simple model and is not intended to be exhaustive. The effects of different shapes, cracks resulting from mechanical damage, and the effects of different albedo materials and different energy deposition depths have been discussed. As well, the justification for using an energy threshold in deriving the minimum-energy orientations has been considered in depth. However, the model does not explicitly take into consideration any specific material properties whatsoever. This formulation was used, as McFadden et al. (2005) did not observe changes in preferred orientations for vastly different materials. This, more then anything else, argues against specific material properties as a controlling factor. While it would be possible to produce a model that takes as a parameter space different minerologies of clast, different sizes of clast, different shapes of clast, and different energy deposition profiles in each of the different sites observed by McFadden et al. (2005), this would be akin to modeling each specific rock observed! Even undertaking this gargantuan task would not guarantee that any more light would be shed on the problem of preferred orientations then in the general case. This does not mean that these material parameters are unimportant and cannot have significant effects for individual rocks, particularly inasmuch as rates are concerned; however, they do not appear to be controlling in changing the minimum energy orientations.

Finally, where permitted by climate, cracks in rocks can be havens not only for liquid water but also for fine-grained mineral dust and biological organisms. The presence of these actors may enhance the propagation of cracks that are able to grow large enough to admit either of these elements. Beginning with fine-grained material, soils have been seen to enhance weathering. For instance, Barton (1916) recounted observations of enhanced weathering that he attributed to an ancient soil line on granite monuments in Egypt. This makes sense as fine-grained material will have a low thermal inertia, thus protecting lower layers from being baked out and preserving water for long periods of time in pore space and in contact with the walls of the rock. This process promotes weathering and can even loosen mineral grains from the rock, which then become a part of the sediment in the crack (Certini et al., 2002). Retention of moisture by organisms (including plants, algae and lichen) can also help to enhance cracking along preferred directions. In fact, in more arid climates, the growth of lichens in preferred environments, such as shielded cracks, can be a major cause of granular disintegration (Guglielmin et al., 2005).

4.2. Thermal cycling vs. differential insolation: application to other environments and solar system bodies

Can differential solar insolation be expected to be a significant factor in breakdown in other arid environments throughout the solar system? Here we consider three examples: the Antarctic Dry Valleys, Mars, and the Moon. These environments provide opportunities to examine the thermal cycling model and test it against the differential-insolation model described here.

An interesting geomorphic possibility can potentially be found in polar arid regions, such as the Antarctic Dry Valleys. In areas such as these, strong gradients in temperature of rocks are possible that

overlap with the freezing point of water (Hall and Hall, 1991). As such, cracks with low amounts of insolation may not propagate most easily, but instead those cracks that receive the most insolation and are thus able to mobilize any internal water for a significant part of the year.

This is an especially pertinent case as there is a significant body of work analyzing the thermal state of rocks in polar regions (Hall, 1997,1998; Lewkowicz, 2001; Hall and André, 2003). That thermal cycling could contribute to the breakdown of rocks is a natural assumption (for instance, Ishimaru and Yoshikawa, 2000) in areas known for significant freeze-thaw weathering and where permafrost has been seen to repeatedly fracture upon thermal contraction to form polygons. However, in those areas containing clasts made of consolidated rock and with ample sunlight, differential insolation may apply as well, especially if the cracking that occurs is directional in nature (for instance, French and Guglielmin, 2007). As with desert rocks, moisture may play a role as saturated highly porous materials (Mackay, 1999) are seen to fracture easily, whereas freeze-thaw damage is not observed where the moisture content is low (Hall, 1997). Additionally, some researchers have found that rock grains may be more susceptible to damage at lower temperatures (French and Guglielmin, 2000). As polar deserts are much more accessible then Mars or the Moon, they provide an excellent place to test thermal cycling against differential insolation.

Secondly, Mars possesses a significant daily thermal range, a thin atmosphere, and at least occasionally has liquid water available at the surface (Malin et al., 2006). As well, erosive processes that do occur are slow as evidenced by the significant cratering of the entire planet at all scales (Strom et al., 1992). As such, rocks may sit on the surface undisturbed for extremely long periods of time, compared to terrestrial deserts. Also, Mars has been surveyed by numerous Landers and Rovers that have provided a

rich data set of thousands of images for examination. While a comprehensive study of these data products is beyond the scope of this paper, this process may be significant for Mars. Periglacial processes are known to occur at northern latitudes as evidenced by ice polygons (Mangold, 2005), and rocks may exceed the 0°C threshold in summer at equatorial to mid latitudes (Christensen et al., 2001). Water ice frosts have also been observed at mid latitudes by Viking Lander 2 (Wall, 1981).

This suggests that if differential insolation is significant for a dry polar terrestrial location, such as the Antarctic dry valleys, it likely has applications to Mars where water vapor condensed on the inside of rocks may be cycled through heating. Even so, whether this process is significant for Mars may be difficult to determine as it may not be possible to observe rock fabric from the image set and thus screen out this component of cracking. Also, the obliquity of Mars and hence the insolation at any point on the surface varies considerably with time. This oscillation, termed an obliquity cycle, can change the effective angle of the sun for by more then 20° over periods of ~ 10^5 years with larger variations over longer timescales (Laskar et al., 2004), this will need to be taken into account in any simulation of crack propagation.

Lastly, the Moon and other airless bodies are considered. While airless bodies do not provide an environment where differential-insolation cracking can take place, they do provide a place where thermal cycling could play a role. Diurnal temperature variations on the moon are very severe compared to the Earth (Lodders and Fedgley, 1998); as well, without an atmosphere, the insolation contribution by the diffuse sky (especially in the infrared) is zero. As such, if directional fractures appear here similar to those observed by McFadden et al. (2005), it would suggest that thermal cycling is the causative agent.

If there are no directional fractures, then the differential-insolation model described in this paper is more likely to be relevant for the Earth.

5. Conclusions

Numerical modeling of solar insolation in cracks of different orientations and depths show that certain orientations of cracks can receive more insolation then other cracks on all timescales. The pattern of orientations that are favored changes for different depths of cracks under the same conditions. By assuming that crack growth is proportional to moisture content in a crack that is itself inversely proportional to the received insolation on the crack bottom, the orientations that would propagate most rapidly were determined.

For the U.S. southwest, three different modes were exhibited, a N-S population when the initial crack was shallow, an ESE-WNW and ENE-WSW population when initial cracks were of intermediate depth, and an E-W population when initial cracks were deep. The first two modes correlate well to the data retrieved by McFadden et al. (2005) for cracked rocks at several sites in the U.S. southwest. Thus, the pattern of yearly average insolation in selecting certain orientations for growth and not others correlates well with the observed data. The E-W mode predicted by the simulation is not seen and could result from a lack of deep initial cracks compared to shallow cracks and an inability of the discharge of moisture to respond to variations in insolation shorter then a year. This relative lack of E-W cracks compared to ENE-WSW cracks, which are themselves less common then N-S oriented cracks, correlates well with the idea that these modes are associated with progressively shallower initial cracks that are progressively more common in the initial surface cracking of rocks.

The apparent offset in the N-S mode and the lack of an ENE-WSW mode in the data set of McFadden et al. (2005) is also correlated with the diurnal cycle of rainfall in the summer that promotes recharge of certain crack orientations and not others. This suggests that a record of both the annual variation in insolation and the daily pattern of rainfall could be preserved in the orientations of cracks on rocks in the U.S. southwest.

6. Acknowledgements

Partial funding for this work was provided by the Natural Sciences and Engineering Research Council of Canada (NSERC).

7. References

ASTM, 2003. Standard Solar Constant and 1.5 Air Mass Spectral Irradiance Tables, Standard G173-03. American Society for Testing and Materials, West Conshohocken, PA.

Barton, D.C., 1916. Notes on the disintegration of granite in Egypt. Geology 24, 382-393.

Barton, D.C., 1938. Discussion: The disintegration and exfoliation of granite in Egypt. Geology 46, 109-111.

Blackwelder, E., 1933. The insolation hypothesis of rock weathering. American Journal of Science 26, 110.

Bowen, B.M., 1996. Rainfall and climate variation over a sloping New Mexico plateau during the North American monsoon. Journal of Climate 9, 3432-3442.

Certini, G., Corti, G., Ugolini, F.C., DeSiena, C., 2002. Rock weathering promoted by embryonic soils in surface cavities. European Journal of Soil Science 53, 139-146.

Christensen, P.R., Bandfield, J.L., Hamilton, V.E., and 23 co-authors, 2001. Mars Global Surveyor Thermal Emission Spectrometer experiment: Investigation description and surface science results. J. Geophys. Res. 106 E10, 23823-23872.

Clark, V.A., Spencer, T.W., Tittmann, B.R. 1981., The effect of thermal cycling on the seismic quality factor Q of some sedimentary rocks. J. Geophys. Res 86 B8, 7087-7094.

Clifford, S.M., Hillel, D., 1983. The stability of ground ice in the equatorial region of Mars. J. Geophys Res. 88 B3, 2456-2474.

Dunai, T.J., Gonzáles-Lòpez, G.A., Juez-Larré, J., 2005. Oligocene-Miocene age of aridity in the Atacama Desert revealed by exposure dating of erosion-sensitive landforms. Geology 33 4, 321-324; doi: 10.1130/G21184.1.

Fredrich, J.T., Wong, T.-F., 1986. Micromechanics of themally induced cracking in three crustal rocks. J. Geophys. Res. 91 B12,12743-12764.

French, H.M., Guglielmin, M., 2000. Cryogenic weathering of granite, Northern Victoria Land, Antarctica. Permafrost and Periglacial Processes 11: 305-314.

French, H.M., Guglielmin, M., 2007. Cryogenic grooves on a granite nunatak, northern Victoria Land, Antarctica. Norwegian Journal of Geography 56:2, 112-116. doi: 10.1080/002919502760056431.

Gates, D.M., 1980. Biophysical ecology. Springer-Verlag. New York.

Géraud, Y., Mazerolle, F., Raynaud, S., 1992. Comparaison between connected and overall porosity of thermally stressed granites. Journal of Structural Geology, 14 8, 981-990.

Griggs, D.T., 1936. The factor of fatigue in rock exfoliation. Geology 44, 783-796.

Guglielmin, M., Cannone, N. Strini, A. Lewkowicz, A.G., 2005. Biotic and abiotic processes on granite weathering landforms in a cryotic environment, northern Victoria Land, Antarctica. Permafrost and Periglacial Processes, 16, 69-85.

Hall, K., 1997. Rock temperatures and implications for cold region weathering I: new data from Viking Valley, Alexander Island, Antarctica. Permafrost and Periglacial Profcesses 8: 69-90.

Hall, K., 1998. Rock temperatures and implications for cold region weathering II: new data from rothera, Adelaide Island, Antarctica. Permafrost and Periglacial Processes 9: 47-55.

Hall, K., André, M.-F., 2003. Rock thermal data at the grain scale: applicability to grannular disintegration in cold environments. Earth Surface Processes and Landforms 28: 823-836; doi: 10.1002/esp.494.

Hall, K., Guglielmin, M., Strini, A., 2008. Weathering of granite in Antarctica: I. light penetration into rock and implications for rock weathering and endolithic communities. Earth Surface Processes and Landforms 33 295-307.

Hall, K., Hall, A., 1991. Thermal gradients and rock weathering at low temperatures: some simulation data. Permafrost and Periglacial Processes 2, 103-112.

Hapke, B., 1993. Theory of reflectance and emittance spectroscopy (topics in remote sensing). Cambridge University Press.

Iñigo, A.C., Vicente, M.A., Rives, V., 2000. Weathering and decay of granitic rocks: its relation to their pore network. Mechanics of Materials 32, 555-560.

Ishimaru, S., Yoshikawa, K., 2000. The weathering of granodiorite porphyry in the Thiel Mountains, inland Antarctica. Geogr. Ann. 82 A (1): 45-57.

Johnston, D.H., Toksöz, M.N., 1980. Thermal cracking and amplitude dependant attenuation. J. Geophys. Res. 85 B2, 937-942.

Klobes, P., Riesemeier, H., Meyer, K., Goebbels, J., Hellmuth, K.-H., 1997. Rock porosity determination by combination of X-ray computerized tomography with mercury porosimetry. Fresenius J. Anal Chem. 357, 543-547.

Laskar, J. Correia, A.C.M., Gastineau, M., Joutel, F. Levrard, B., Robutel, P., 2004. Long term evolution and chaotic diffusion of the insolation quantities of Mars. Icarus 170 2, 343-364.

Leathers, D.J., Palecki, M.A., Robinson, D.A., Dewey, K.F., 1998. Climatology of the daily temperature range annual cycle in the United States. Climate research 9, 197-211.

Lewkowicz, A.G., 2001. Temperature regime of a small sandstone tor, latitude 80°N, Ellesmere Island, Nunavut, Canada. Permafrost and Periglacial Processes 12: 351-366; doi: 10.1002/ppp.396.

Lodders, K., Fedgley, B. Jr., 1998. The planetary scientist's companion. Oxford University Press, New York.

Mabbutt, J.A., 1977. Desert landforms. MIT Press, Cambridge, Mass.

Mackay, J.R., 1999. Cold-climate shattering (1974 to 1993) of 200 glacial erratics on the exposed bottom of a recently drained arctic lake, western arctic coast, Canada. Permafrost and Periglacial Processes 10: 125-136.

Malin, M.C., Edgett, K.S., Posiolova, L.V., McColley, S.M., Dobrea, E.Z.N., 2006. Present-day impact cratering rate and contemporary gully activity on Mars. Science 314 5805, 1573-1577.

Mangold, N., 2005. High latitude patterned grounds on Mars: classification, distribution and climatic control. Icarus 174 2, 336-359.

McFadden, L.D., Eppes, M.C., Gillespie, A.R., Hallet, B., 2005. Physical weathering in arid landscapes due to diurnal variation in the direction of solar heating. GSA Bulletin 117 1, 161-173.

Moores, J.E., Smith, P.H., Tanner, R., Schuerger, A.C., Venkateswaran, K.J., 2007. The shielding Effect of small scale martian surface geometry on ultraviolet flux. Icarus 192/2, 417-433.

Schild, M., Siegesmund, S., Vollbrecht, A., Mazurek, M., 2001. Characterization of granite matrix porosity and pore-space geometry by in situ and laboratory methods. Geophys J. Int. 146, 111-125.

Simmons, G., Cooper, H.W., 1978. Thermal cycling cracks in three igneous rocks. Int J. Rock Mech. Min. Sci. & Geomech. Abstr. 15, 145-148.

Sprague, A.L., Hunten, D.M., Doose, L.R., Hill, R.E., Boynton, W.V., Smith, M.D., Pearl, J.C., 2006. Mars atmospheric water vapor abundance: 1991-1999 emphasis 1998-1999. Icarus 184, 372-400.

Strom, R.G, Croft, S.K., Barlow, N.G. 1992. The martian impact cratering record, in Mars, edited by Jakowsky, B.M. et al., 383-423. University of Arizona Press, Tucson, Arizona.

Tomasko, M.G., Moores, J.E., Smith, P.H., and 39 co-authors, 2005. Rain, winds and haze during the huygens probe's descent to Titan's surface. Nature 438 7069, 765-778.

Tucker, D.F., 1993. Diurnal precipitation variation in south-central New Mexico. Monthly Weather Review 121, 1979-1991.

Wall, S.D., 1981. Analysis of condensates formed at the Viking 2 lander site – the first winter. Icarus 47, 173-183.

Figure Captions:

Fig. 1. 10° binned rose diagram of crack orientations unrelated to local conditions or rock fabric after McFadden et al. (2005) using the frame of reference as described in this publication with North indicated at 0°. The cracks are oriented with two major modes represented, a primary N-S mode and a weaker ENE-WSW mode.

Fig. 2. Geometry of the simulated cracks with aspect ratios of 8:1:1 (A) and 8:1:3 (B). Both cracks are shown in an E-W configuration corresponding to a rotation angle of 90°. The direction of increasing rotation angle is shown in both panels and is consistent with the frame of reference shown in Fig. 1.

Fig. 3. Recharge and discharge rates from convoluted 10 cm length capillary pores according to Eqs. [2] and [6], respectively, for a constant crack temperature of 20°C and a relative humidity of 0%. The rates of recharge and discharge are similar for small pores, but drastically different for large pores because of the transition between the Knudsen and molecular diffusion regimes.

Fig. 4. Daily variation in insolation for cracks of different orientations at 35° N. on 21 March for (A) a shallow crack with an aspect ratio of 8:1:1 and (B) a deeper crack with an aspect ratio of 8:1:4. As the crack deepens, the range of orientations that receives insolation at any one time decreases.

Fig. 5. Insolation by season for the cracks shown in Fig. 3. Note that only 0-90° are displayed as the path of the sun in the sky is symmetric. “Winter” behavior is exhibited by three of eight L_S at a depth of one unit, but seven of eight L_S behave in this way at four units of depth.

Fig. 6. Annual insolation on cracks divided into three regimes. Cracks with a minimum in insolation at N-S orientations (A), cracks with a minimum in insolation away from E-W or N-S (B), and cracks with a minimum at E-W orientations (C). Open squares and circles indicate the identity of the line; resolution is 1°.

Fig. 7. Rose diagrams of preferred orientations for water retention corresponding to the three regimes shown in Fig. 6. Depending upon the depth, cracks may be produced with any of the three forms. Panel A corresponds to a crack depth of 0.2, panel B to 1.5, and panel C to 4.0. The energy thresholds used were 1.65×10^{9} J y^{-1} m^{-2}, 4.70×10^{8} J y^{-1} m^{-2}, and 1.12×10^{8} J y^{-1} m^{-2} for each panel, respectively. Cracks that receive more energy then this threshold are considered baked out and are not shown.

Fig. 8. Cumulative insolation by 1320 at Los Alamos, NM, by crack orientation. ENE-WSW cracks receive less insolation by the early afternoon compared to WNW-ESE trending cracks at all depths of the initial crack. The differential is more extreme for the variation shown in Fig. 6, panel C (120° vs 60°) then for panel B (20° vs 170°). Open squares and circles indicate the identity of the line; resolution is 1°.

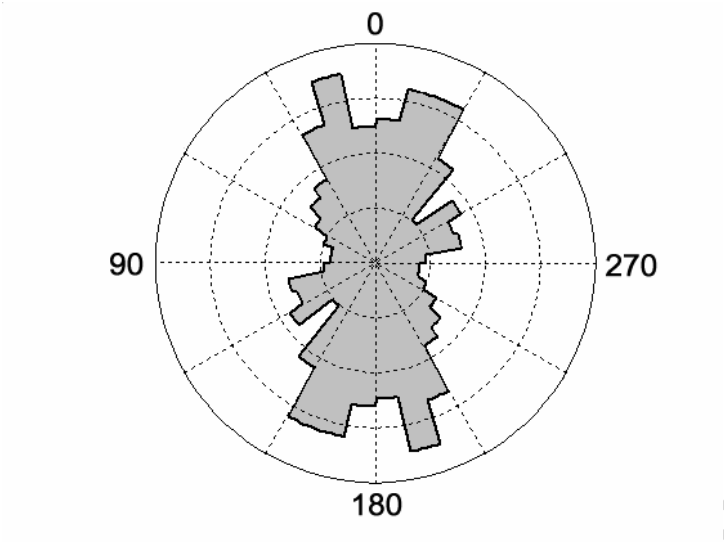

Fig. 1

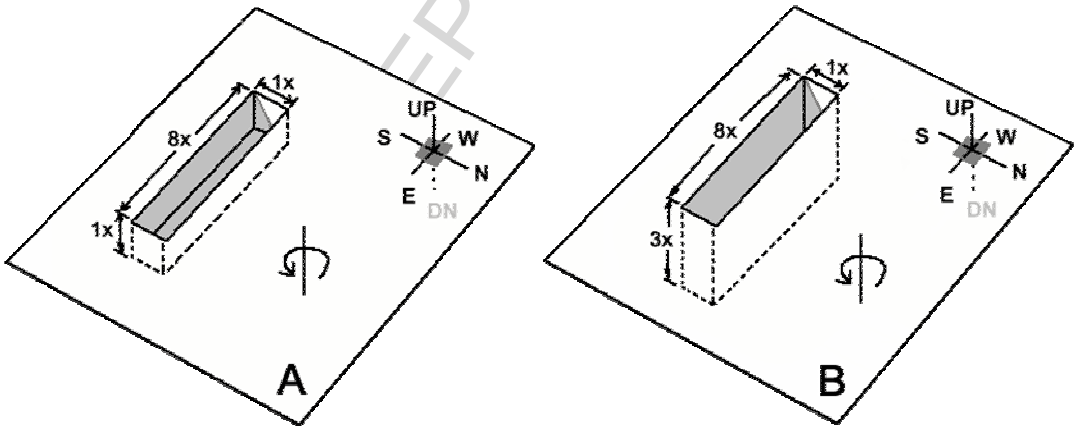

Fig. 2

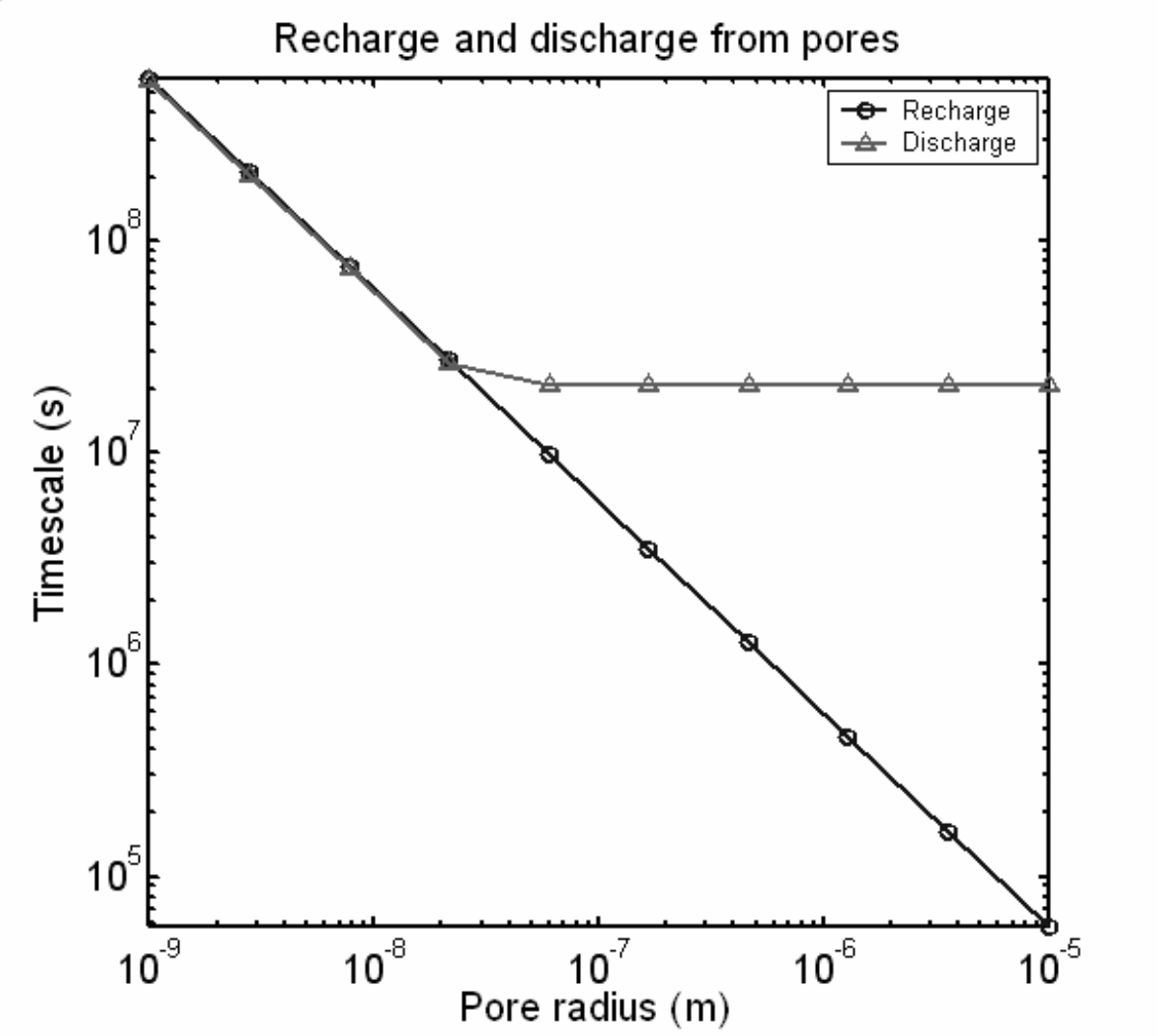

Fig. 3

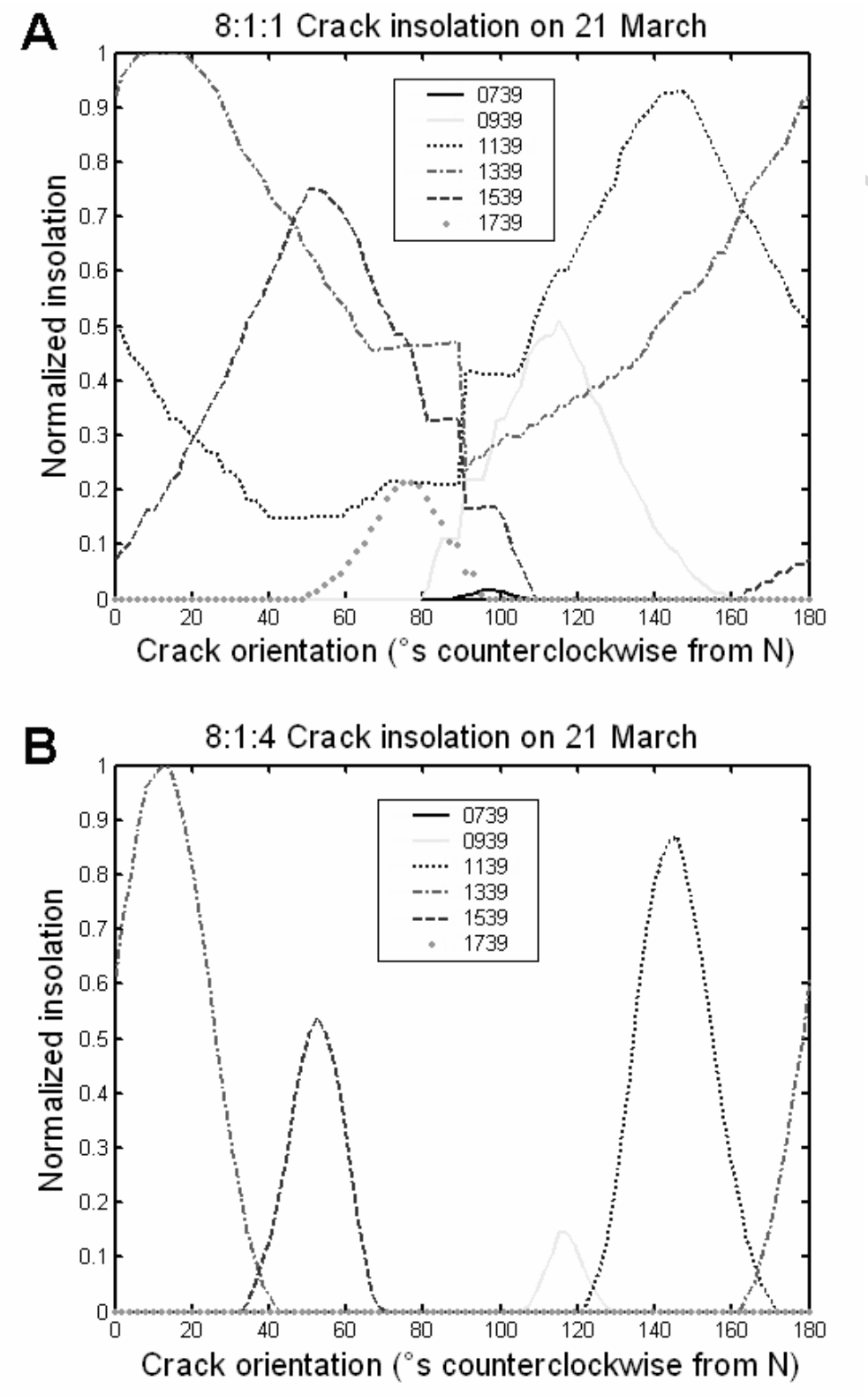

Fig. 4

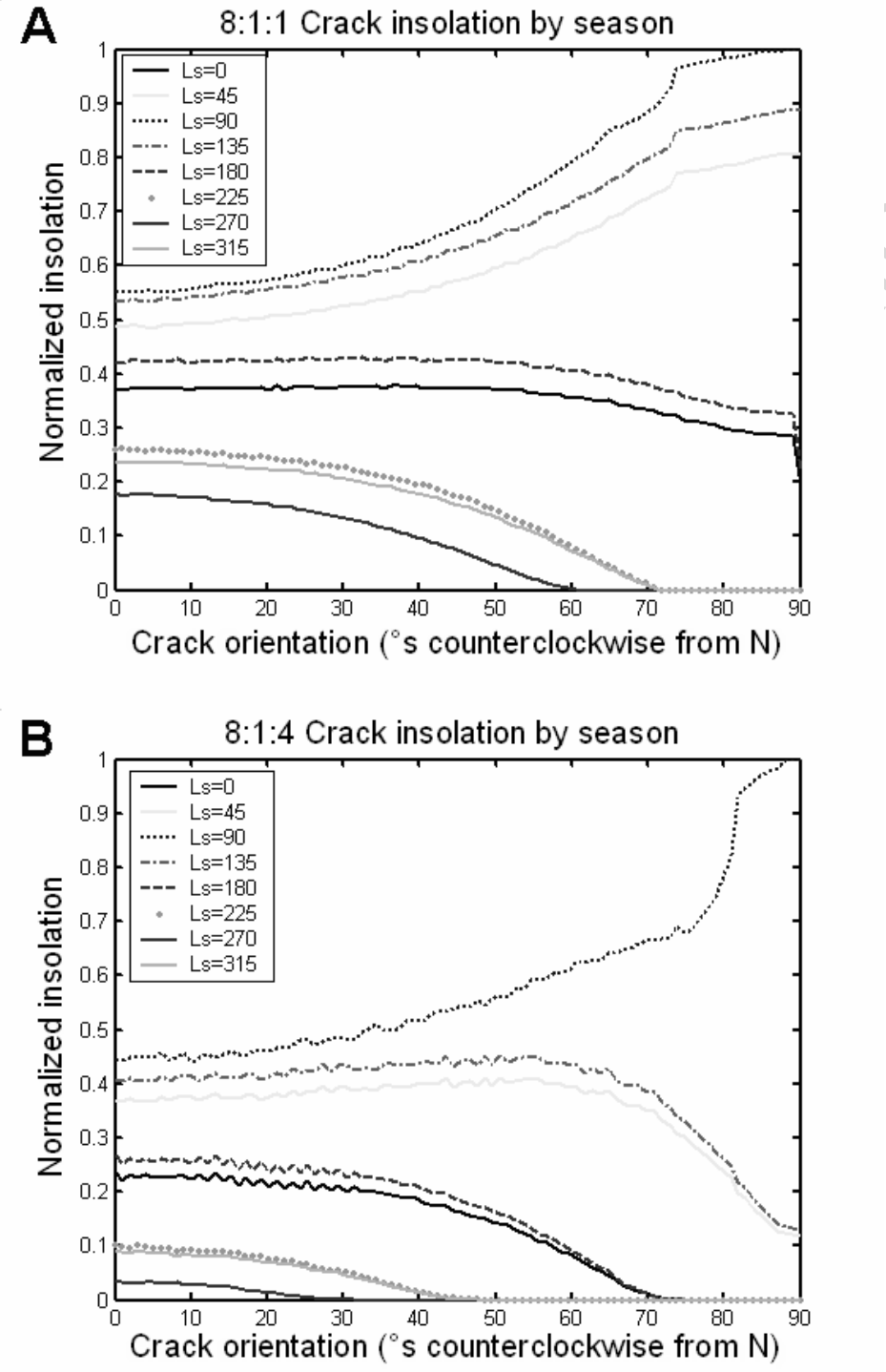

Fig. 5

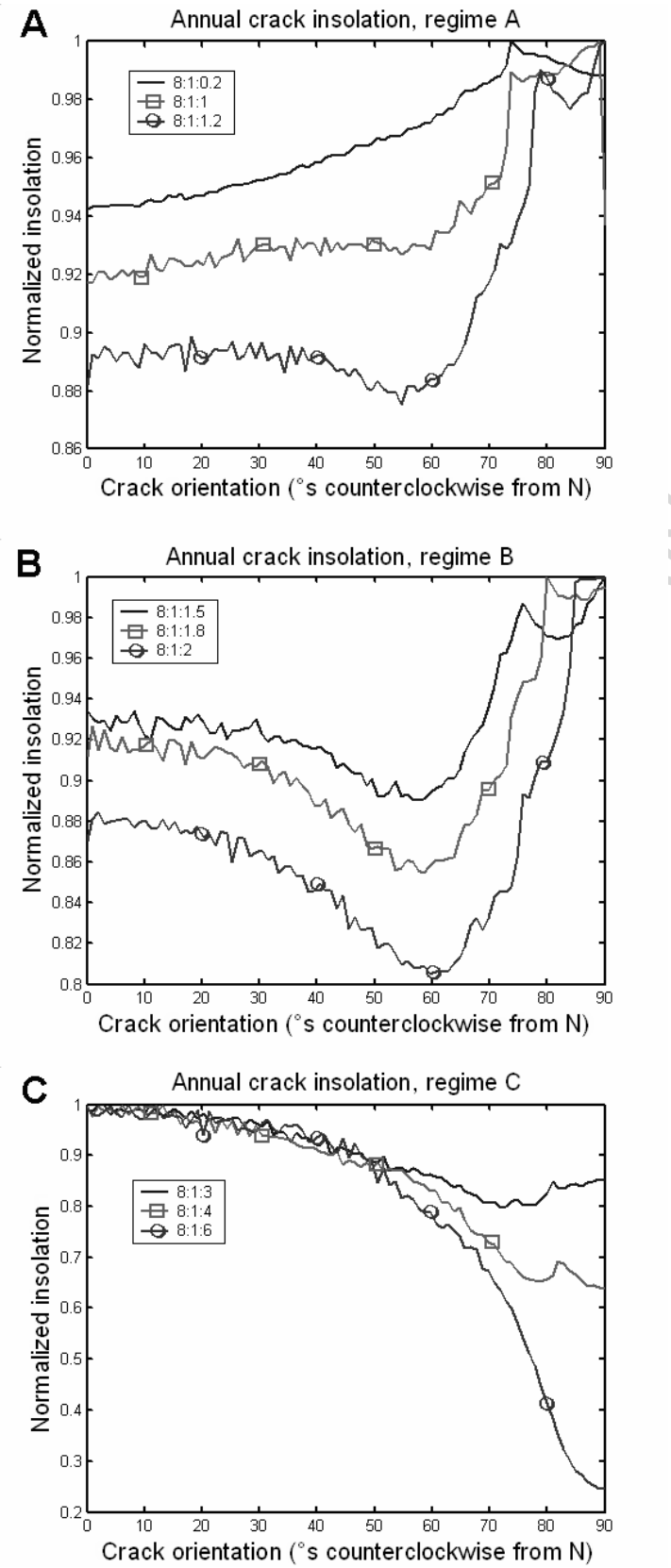

Fig. 6

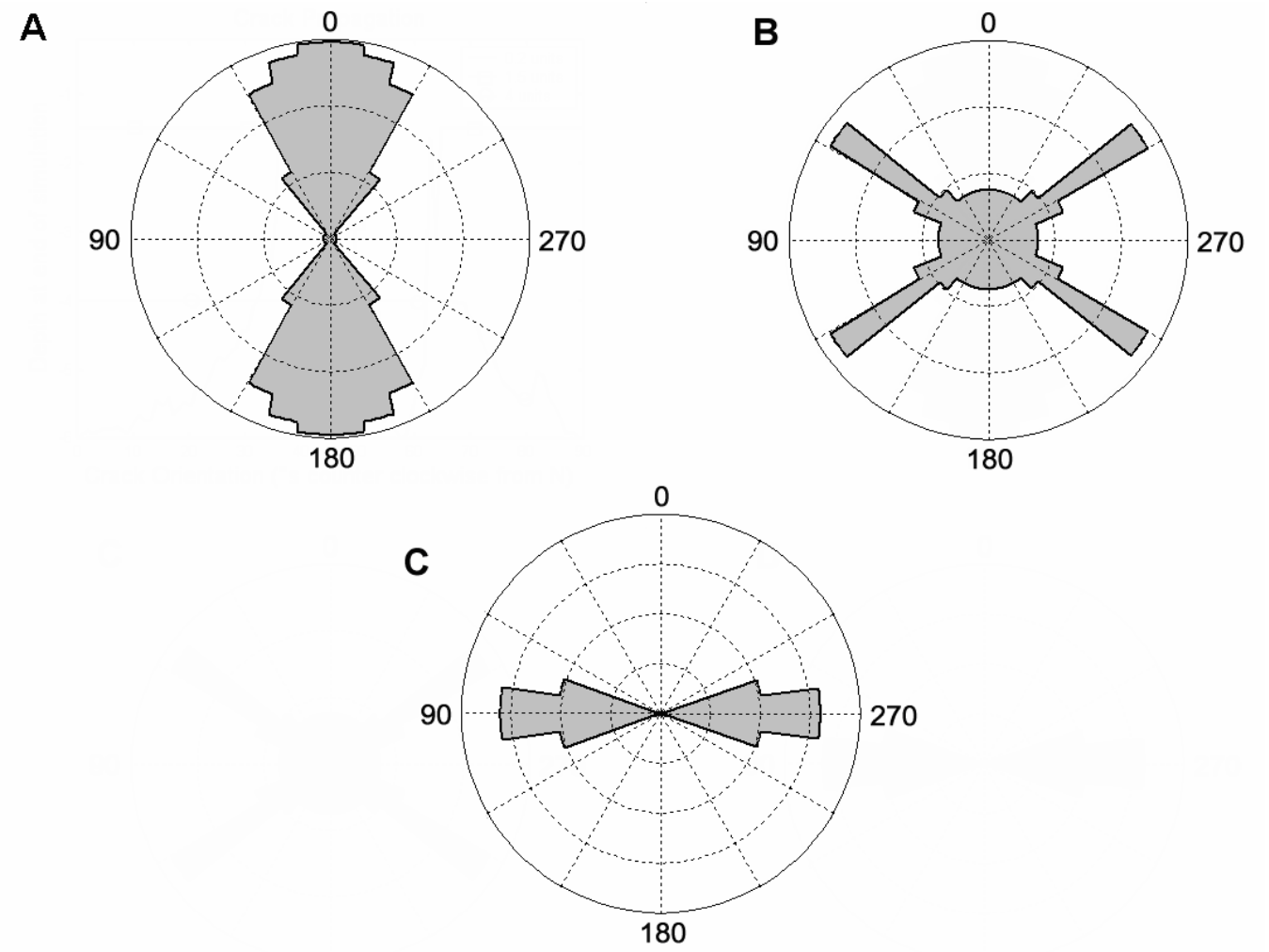

Fig. 7

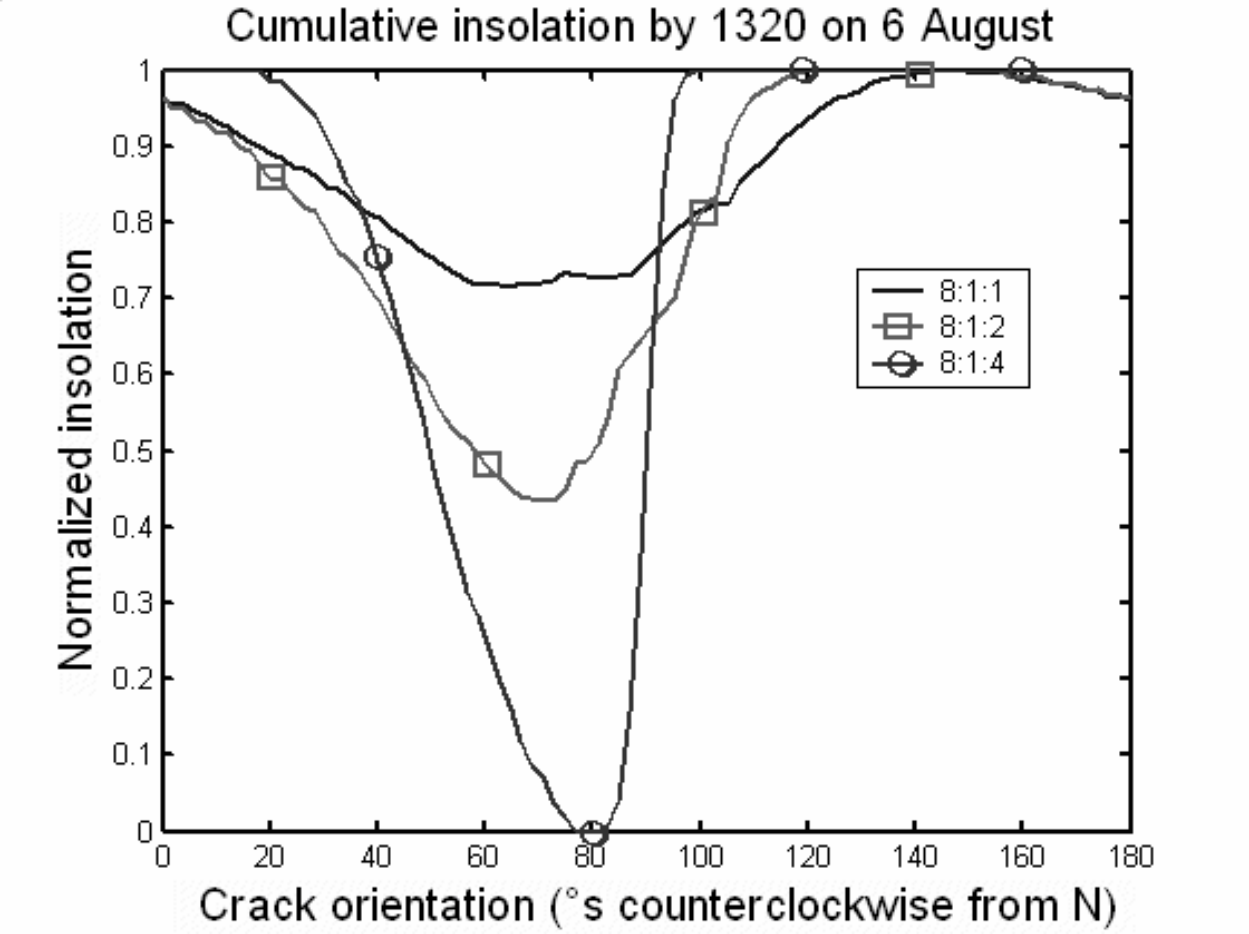

Fig. 8